Low pressure plasma nitrided CoCrMo alloy utilising HIPIMS discharge for biomedical applications

KRISHNANAND, Shukla, ARUNACHALAM SUGUMARAN, Arunprabhu <http://orcid.org/0000-0002-5087-4297>, KHAN, Imran, EHIASARIAN, Arutiun and HOVSEPIAN, Papken

Published version

KRISHNANAND, Shukla, ARUNACHALAM SUGUMARAN, Arunprabhu, KHAN, Imran, EHIASARIAN, Arutiun and HOVSEPIAN, Papken (2020). Low pressure plasma nitrided CoCrMo alloy utilising HIPIMS discharge for biomedical applications. Journal of The Mechanical Behavior of Biomedical Materials.

Low pressure plasma nitrided CoCrMo alloy utilising HIPIMS discharge for biomedical applications

Krishnanand Shukla[1*], Arunprabhu A. Sugumaran[1], Imran Khan[2], A. P. Ehiasarian[1], P. Eh Hovsepian[1]

[1] National HIPIMS Technology Centre UK, Materials and Engineering Research Institute, Sheffield Hallam University, Sheffield, S1 1WB, UK.

[2] Zimmer-Biomet UK Limited, Dorcan Industrial Estate, Murdock Road, Swindon SN3 5HY, UK.

* Corresponding author: krishnanand.shukla@student.shu.ac.uk

Abstract

CoCrMo is a biomedical grade alloy which is widely used in the manufacturing of orthopaedic implants such as hip and knee replacement joints because of it has high hardness, high corrosion resistance, and excellent biocompatibility. However, the release of metal ions due to corrosion and wear of the alloy over time may cause allergic or other adverse reactions in some patients. To date, various surface modification techniques including nitriding, have been used to improve the performance of CoCrMo (F75) alloy.

In the current work, a new low-pressure plasma nitriding process is described. Unlike conventional plasma nitriding, the process utilises High Power Impulse Magnetron Sputtering (HIPIMS) discharge, sustained on one Cr target at low power, to further enhance the ionisation of the gas in the vacuum chamber and to avoid coating deposition. The nitriding of CoCrMo alloy has been carried out in a wide range of nitriding voltages (from -500 V to -1100 V) at 400 °C for duration of 4 hours. The chemical and phase composition of the nitrided layer has been studied by various advanced surface analyses techniques.

The X-ray diffraction data of all the nitrided samples revealed the formation of expanded austenite (γN) phase. Texture analyses revealed that at lower nitriding voltages (-700 V) the predominant crystallographic orientation of the compound layer is (200) whereas at higher voltages (-900 V to -1100 V) the layer develops mixed (111) and (200) texture. For samples nitrided at a lower bias voltage of - 500 V, diffraction peaks for CrN/NbN and Cr_2N were also observed due to the deposition of target materials (Cr and Nb). However, no coating deposition on the substrate surface was observed at higher bias voltages (-700 V and higher) due to sufficient re-sputtering effect. The results obtained from glow discharge optical emission spectroscopy (GDOES) depth profiling showed that the depth of nitriding increased from approximately 0.7 µm at -500 V to 6 µm at -1100 V. In the pin-on-disc tribological test nitrided samples showed low coefficient of friction µ in the range of 0.6 to 0.7, compared to µ= 0.8 recorded for the untreated substrate. The wear coefficients (Kc) were found to be between 1.79×10^{-15} $m^3N^{-1}m^{-1}$ (-700 V) and 4.62×10^{-15} $m^3N^{-1}m^{-1}$ (-1100 V), which were one order of magnitude lower than the untreated substrate, Kc = 6×10^{-14} $m^3N^{-1}m^{-1}$. The Knoop microhardness (HK) of nitrided samples significantly increased by a factor of 5 (HK= 2750 at -1100 V) as compared to the untreated substrate, HK=525, demonstrating the high efficiency of the process. The samples nitrided at -700 V and - 900 V exhibited enhanced corrosion resistance as compared to untreated alloy by avoiding the formation of CrN based compounds which adversely affect the corrosion performance.

Keywords: Biomaterials; Surface Engineering; Diffraction; GDOES; Simulated Body Fluid (Hank's Solution).

1. Introduction

CoCrMo (ASTM-F75) is a biomedical grade alloy with high fatigue, tensile strength and enhanced corrosion resistance [1-3]. It is mainly used as a femoral head in total hip replacement and femoral component in total knee replacement implants [3]. However the lifetime of these implants can be impacted by various factors, including wear [4] and the release of metal ions due to tribocorrosion [5]. The release of metal debris/ions may induce dose-dependent adverse biological reactions in the periprosthetic tissues of some patients and may also transfer through blood to different parts of the body [5-6]. Patient-related factors can also influence wear and corrosion of implant surfaces, as these mechanisms can be significantly accelerated due to high cyclic loading [7].

Over the years, various surface hardening techniques including plasma nitriding, plasma carburizing [13], high intensity plasma ion nitriding [10-11] and plasma immersion ion implantation nitriding [12] have been used to overcome the above described drawbacks. It has been found by many researchers that plasma nitriding and carburising of CoCrMo alloy at low temperature can form duplex nitrided layers (compound and diffusion) or S-phase without forming any CrN precipitation layer [14-16] thus enhancing the mechanical and tribological behaviour of the base material. It has been first observed by Zhang et. al. that the hardness of the austenitic steel (AISI 316) can be improved by nitriding without altering the intrinsic corrosion resistance of the substrate [17]. In the case of CoCrMo alloy, the formation of expanded austenite phase at low temperature carburising has shown better wear resistance with no loss of corrosion resistance [18] in tribocorrosion conditions in both air and Ringer's solution [5]. Hutchings et. al, also found that the wear resistance of nitrided Ti alloy increased two

orders of magnitude as compared to an untreated substrate [19]. Wei Ronghya et.al reported that low ion energy ion implantation at elevated temperatures that produced a thick nitride layer resulted in improved tribological properties. They have also found that the case depth increased as ion energy increased [20]. However, many researchers have reported that the oxide layers present on the surface of the substrate can act as a barrier in achieving high nitriding depth [21-24].

Hovsepian et al. have successfully demonstrated that it was possible to nitride austenitic stainless steel at low pressure (in the range of 10^{-3} mbar,) using High Power Impulse Magnetron Sputtering (HIPIMS) discharge. The advantage of using HIPIMS for nitriding is that it can generate highly ionised plasma which dramatically enhances the process efficiency due to the utilisation of the ion irradiation enhanced diffusion processes. Another motivation behind the development of low pressure nitriding process (in the 10^{-3} mbar range, which is three orders of magnitude lower than that of the conventional glow discharge process) is the significant reduction of the negative effect of the oxygen ions on the nitrogen diffusion and the possibility to execute it in a standard physical vapour deposition (PVD) type equipment. This is seen as very advantageous approach as it allows duplex type of treatment of the surface involving enhancement of substrate load bearing capacity by plasma nitriding followed by an application tailored PVD top coating in one PVD system.

In the present study, CoCrMo alloy (F75) was plasma nitrided using HIPIMS discharge at low pressure. The degree of ion bombardment was varied by varying the bias voltage applied on the treated substrate in the range from -500 V to -1100 V. Other process parameters such as temperature, operating pressure and process time were kept constant. The effect of substrate bias on nitriding depth, mechanical and tribological properties were extensively studied and compared to those of untreated CoCrMo alloy and treated in standard plasma nitriding process which utilises direct current glow discharge.

2. Experimental Details

2.1 Materials and Methods

CoCrMo (ASTM F75) alloy with chemical composition as listed in Table 1 was used as substrate material (sample dimensions: Ø 16 mm x 5 mm). Prior to loading into the chamber, samples were mirror polished (1 μm diamond paste) and cleaned in an automated industrial size cleaning line containing several baths with different industrial detergents, (alkali solutions), deionised water and ultrasonic agitation to remove all contaminants from the surface (mostly organic contaminations such as oils). The degreased samples were dried in a vacuum drier at 120 °C for 30 minutes.

Element	% mass/mass
Cr	27 – 30
Mo	5 – 7
Ni	≤ 0.5
Fe	≤ 0.75
C	≤ 0.35
Si	≤ 1.0
Mn	≤ 1.0
Tu	≤ 0.2
P	≤ 0.20
S	≤ 0.10
N	≤ 0.25
Al	≤ 0.1
Ti	≤ 0.1
B	≤ 0.1
Co	Balance

Table 1: Chemical composition of CoCrMo alloy (F75)

HIPIMS enhanced low-pressure plasma nitriding (HLPPN) was carried out in an industrial size PVD machine (Hauzer techno Coating 1000-4, The Netherlands) enabled with HIPIMS technology at Sheffield Hallam University. The system is equipped with two (Hüttinger Elektronic sp z o. o.) power supplies and a specialised HIPIMS compatible bias power supply with arc suppression unit, [25]. Both the cathode and bias power supplies were operated in voltage-controlled mode, whereby the voltage was maintained constant with an accuracy of 5% of the setpoint by supplying the required current. The bias voltage was kept at a dc level and the cathode voltage was pulsed. The substrates were mounted on special holders on a rotating table, located at the centre of the chamber, which can allow three-fold rotation. Prior to the plasma nitriding, the substrate surface was pre-treated by HIPIMS plasma discharge (enriched with Ar and Cr ions) to remove any kind of residual organic contaminants and oxide layers from the surface. During this step, the surface is subjected to intensive bombardment by Cr+ ions generated by HIPIMS discharge on a Cr target [25,26]. The nitriding was carried out in a mixed N_2/H_2 (85:15) atmosphere by maintaining HIPIMS discharge on one pair of Cr and Nb targets and unbalanced magnetron sputtering (UBM) discharge maintained on a second pair of Cr and Nb targets for 4 hours. The reactive gas flow rate was precisely controlled using plasma emission monitoring and control system "Speedflo" manufactured by Gencoa Ltd. UK. The bias voltage was varied from -500 V to -1100 V in order to provide ion bombardment at different energies. The substrates were biased by a generator operating in voltage-controlled mode. Time-resolved measurements of the substrate bias voltage using an oscilloscope confirmed that the voltage at the substrate is within 1% of the set voltage and is maintained throughout the power pulse on the magnetrons. No significant change in substrate current was observed for different voltages confirming that the plasma is primarily generated at the magnetron cathodes.

The temperature and the total pressure were kept constant at 400 $^{\circ}$C and 8.3 x 10^{-3} mbar respectively.

2.2 Characterisation techniques

The microstructure, mechanical and tribological properties of the nitrided samples were characterised using a range of highly precise and advanced analytical instruments.

- Phase composition of all treated and untreated CoCrMo was obtained from an Empyrean X-ray diffractometer with *Cu Kα* radiation (1.5418 Å). The Texture coefficient of the nitrided CoCrMo alloy was investigated using glancing angle incidence mode (2^0) and θ-2θ geometry [28].
- An Olympus optical microscope was used to investigate the microstructure and nitriding thickness of all the treated and untreated samples.
- Quantitative elemental depth analysis was performed using Glow Discharge Optical Emission Spectroscopy (GDOES) (*Jobin Yvon*).
- The nitrided layer thickness was investigated using Scanning Electron Microscope (*FEI Quanta 650 3D DualBeam FIB FEG-SEM*) equipped with a secondary electron detector.
- Cross-section SEM analysis were carried out on specially prepared samples. Small sections from the analysed material were cut and moulded together. These sections were further polished to 1µm using diamond paste and chemically etched using a mixture of hydrogen peroxide (H_2O_2) and hydrochloric acid (*HCL*) (*Marble's reagent)* for 16 sec [29].
- A Knoop micro-hardness tester (*Mitutoyo, Microhardness tester*) was used to obtain the hardness of the nitrided samples.

- Surface roughness was characterised by a profilometer (*DEKTAK 150*). The scan size was fixed for 1000 µm (120 sec.) with a resolution of 0.033 µm and the surface roughness (Ra) was calculated based on an average of 3 scans.
- A Dry sliding pin-on-disc (POD) test (*CSM Tribometer*) was used to obtain the coefficient of friction (COF) and coefficient of wear (Kc). All tests were performed at a total sliding distance of 2 km and a rotational speed of 10 cm/s. These tests were carried out at room temperature of about 26 °C and 25% relative humidity. An Al_2O_3 ball with a diameter of 6 mm was used as a counterpart for each test with a fixed load of 5 N.
- Potentiodynamic polarization tests were conducted to study the corrosion performance of the untreated and nitrided specimens in Hank's solution. The test specimens were masked with lacquer to expose a surface area of 1 cm^2. The applied potential was varied from - 1000 mV to +1000 mV with the scan rate of 1 mV/s using a computer controlled Gill-AC potentiostat manufactured by ACM instruments. A saturated Ag/AgCl electrode was used as the reference electrode.

3. Results and discussion

3.1 X-ray Diffraction analysis

The phase composition of the nitrided layers and the untreated surface was investigated by glancing angle x-ray diffraction (GAXRD) at 2° incident angle (Fig 1). XRD data of the untreated CoCrMo substrate showed a predominantly face-centred cubic (FCC) structure, called γ austenite phase (PDF No: 01-071-4651) with peaks around 44.5° and 51.4° along with a hexagonal closed-packed (HCP) structure, called ε phase (PDF No: 04-004-4360). It has been reported that both FCC and HCP structures coexist in CoCrMo alloys. However, generally at room temperature the FCC structure is predominant [30].

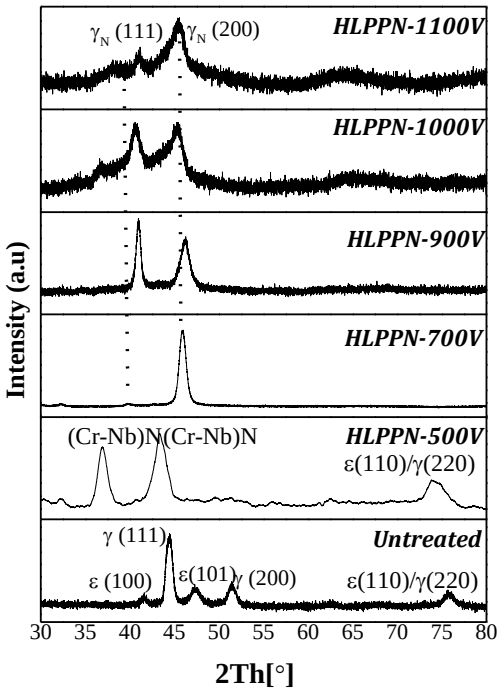

Figure 1: X-ray diffraction data of untreated and nitrided samples at various bias voltages.

In the case of HLPPN-500 V, the XRD pattern showed the (111) and (200) reflections of the FCC structured CrN/NbN at 36° and 42° respectively, as well as a reflection from Cr_2N at 62.5°. This analysis revealed that at low nitriding voltage (- 500 V), a thin (Cr-Nb)-nitride layer was deposited on the sample surface despite intensive re-sputtering of the bombarded surface. It can be stated however that at - 500 V, a nitrided layer is also formed, as revealed by the presence of a higher angle substrate diffraction peak at around 75°, which corresponds to the ε (110)/ γ (220) phase mixture

On the other hand, samples treated at higher bias voltages (from -700 V to -1100 V) showed γ_N (111) and γ_N (200) peaks corresponding to an expanded austenite phase which are shifted to lower 2θ angles compared to the as polished untreated substrate. This shift is mainly due to the expansion of the FCC lattice by the insertion of nitrogen in the

octahedral sites of such structure during nitriding, even though residual stress and stacking faults can also cause such lattice expansion. It is important to note that the XRD data of HLPPN-1000V and HLPPN-1100V also showed traces of CrN and Cr_2N compounds unlike HLPPN-700V and HLPPN-900V samples. It has been already reported that the precipitation of chromium nitride compounds was observed when the nitriding was carried out at 520 °C [31]. In this research, during the nitriding of HLPPN-1000V and HLPPN-1100V samples, the actual process temperature increased up to 510 °C because of the intense ion bombardment due to high bias voltages, even though the set value was much lower of about 400 °C. In the case of HLPPN-700V and HLPPN-900V samples, the actual process temperature was around 430 °C, hence no chromium nitride compound precipitation. Table 2 shows peak position, the calculated interplanar distance (d), lattice parameter (a) and lattice expansion ($\frac{\Delta a}{a_0}$) of the (111) and (200) phase of the various (nitrided and untreated substrate) samples. The (111) peak in the sample nitrided at -1100 V exhibited a maximum shift of about 3.5° and the (200) peak in the -900 V sample showed about a 6° shift as compared to the substrate peaks. In the [111] direction, the lattice parameter (a) increased significantly from 0.368 nm to 0.384 nm while increasing the bias voltage from -700 V to -1000 V. However, it decreased to 0.370 while further increasing the bias voltage to -1100 V. It is important to highlight that the lattice parameter (a) for austenite cubic (111) phase in equilibrium state is 0.374 according to the Cobalt-Nitrogen (Co-N) phase diagram. The highest lattice expansion,$(\frac{\Delta a}{a_0})$ of 9.40 % was observed for samples treated at -1000 V as compared to the untreated sample. Therefore, it can be argued that lattice expansion has reached saturation point at -1000 V. In [200] direction, the maximum lattice expansion was found to be 12.99 % for the sample treated at -1000 V as compared to the untreated sample.

The lattice expansion, $(\frac{\Delta a}{a_0})$ in [200] direction was found to be higher as compared to [111] direction for all nitrided samples. Similar behaviour was observed by Ozturk et al. [32] for 316 stainless steel alloy. The sample treated at - 1100 V exhibited the highest difference of about two-fold while comparing the lattice expansion in [111] and [200] directions.

Texture coefficient, (T*) was calculated using the following equation, [28]:

$$T^* = \frac{I_{hkl}/R_{hkl}}{(1/n)\sum_0^n (I_{hkl}/R_{hkl})}$$

Where I(hkl) is the measured peak intensity from the (hkl) reflections, R(hkl) is the reference standard (random) peak intensity from the (hkl) reflections and n is the number of reflections considered. The results from these calculations for all nitrided samples are listed in Table 2. The texture analyses revealed that at a lower bias voltage of -700 V, the predominant crystallographic orientation of the nitrided layer is (200) whereas at higher bias voltages (from -900 V to -1100 V), the layer developed mixed (111) and (200) texture.

Sample ID	**2θ°**		**d (nm)**		**a (nm)**		$\frac{\Delta a}{a_0}$***100 (%)**		**T*(%)**	
	γ_N **(111)**	γ_N **(200)**	**(111)**	**(200)**	**(111)**	**(200)**	**(111)**	**(200)**	**(111)**	**(200)**
Untreated	γ (44.53)	γ (51.43)	0.203	0.177	0.351	0.354			-	-
HLPPN-700V	39.84	45.88	0.213	0.197	0.368	0.394	5.10	11.29	1.51	98.48
HLPPN-900V	40.91	46.17	0.220	0.196	0.381	0.392	8.56	10.73	43.54	56.45
HLPPN-1000V	40.57	45.05	0.222	0.200	0.384	0.4	9.40	12.99	33.83	66.16
HLPPN-1100V	41.05	45.32	0.214	0.199	0.370	0.398	5.41	12.42	28	72

Table 2 : d spacing, T* and lattice parameter of untreated, and HLPPN at different bias voltage: -700V, -900V, -1000V and -1100V.

3.2 Elemental Depth Analysis

Generally, duplex nitrided layers such as diffusion layer (Co_4N) and compound layer ($Co_{2-3}N$) are formed during the nitriding of CoCrMo alloy [14], [33]. According to the Co-N equilibrium phase diagram, at 400 °C, Co_4N is formed when the concentration of N is about 20 at. %. Further increase in the nitrogen concentration will lead to the formation of other under-stoichiometric Co based nitrides such as Co_3N and Co_2N followed by the stoichiometric CoN when the concentration of N is 50 at. % [33]. The elemental depth profiles of treated samples obtained using glow discharge optical emission spectroscopy (GDOES) are depicted in Fig. 2 (a-b). Generally, nitrogen depth profile exhibits plateau-type shapes with sharp leading edges [14]. For samples treated at higher bias voltages (from -700 V to -1100 V), initially, the concentration of nitrogen was about 40 at. % and stable up to a certain depth which then gradually decreased to the lowest value before remaining almost constant.

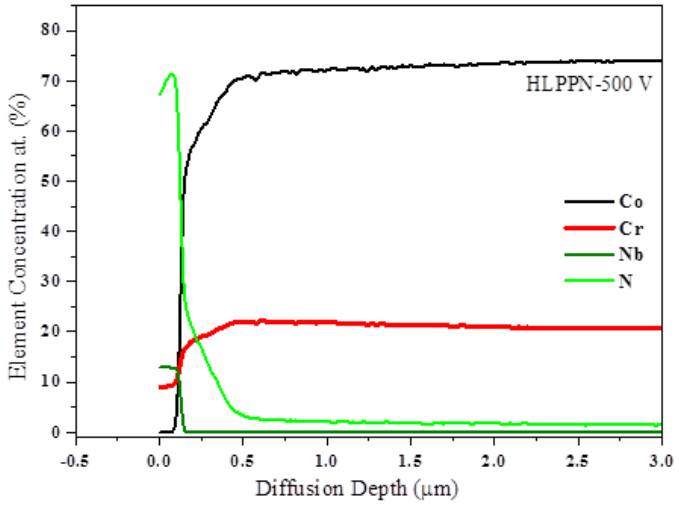

Figure 2a: Elemental depth profile of nitrided sample at -500 V bias voltage.

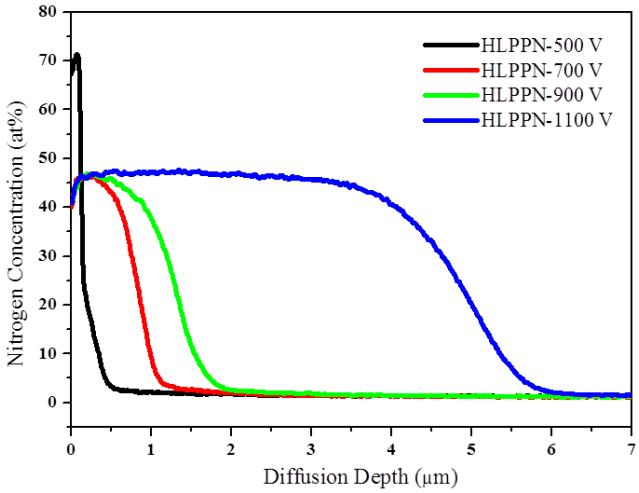

Figure 2b: Nitrogen depth profiles of nitrided samples at various bias voltages.

The diffusion depth was found to be increased while increasing the bias voltage from -700 V to -1100 V. It has been reported that the optimum energy needed to form a deep nitrided layer was of about 1 keV. In this study, the sample with the highest bias voltage of 1100 V (1.1 keV) showed the maximum diffusion depth of about 6 µm. At this energy level, the density of N_2^+ and N^+ ions was found to be increased threefold as compared to 0.5 keV as evidenced by the corresponding increase in substrate bias current. Constant currents and voltages at the cathodes indicated a constant plasma density was generated in the chamber. The substrate bias currents (both average and peak) were proportional to the bias voltage due to the increased area of collection by each sample associated with an increased sheath width. The data confirms our earlier plasma density measurements in the same operating range [35]. Additionally, the intensive ion bombardment generates defects on the surface for these ions to diffuse faster, (ion irradiation enhanced diffusion). The dissociation of neutral N_2 into ions was also achieved by igniting Cr and Nb targets

using HIPIMS/UBM sources at low power densities. The diffusion depth of the other two samples with bias voltages of -700 V and - 900 V was 1.2 µm and 2 µm respectively.

The formation of these layers can be explained by the diffusion model proposed for stainless steel by Williamson et al. [36] due to the similarity of CoCr to stainless steel [37]. According to this model, the Cr atoms act as trapping sites for N and inhibit the diffusion until all Cr trap sites are occupied, resulting in a nitrogen rich compound layer. Subsequently, further incoming N diffuses freely through the compound layer into the substrate, producing transition and diffusion zones, respectively. Also, this model was further refined by Parascondola et al. [38] which included a thermal detrapping mechanism of N from trap sites with detrapping activation energy of 1.45 eV. Akvile Petraitiene et al. adapted this model for CoCr which consisted of nitrogen adsorption on the surface, nitrogen concentration dependent diffusion coefficient of nitrogen and alloy's swelling processes.

The sample treated at -500 V showed a slightly different (very thin plateau) profile with highest nitrogen concentration of about 70 at. % up to ~200 nm depth which then sharply decreased to 25 at. % before gradually reducing to the lowest level shown in Fig. 2a. Notably, the concentration of Cr increased sharply up to 18 at. % before following the similar trend observed for the other treated samples. Also, it is important to highlight that the concentration of target material, Nb, was found to be approx. 13 at. % in this region unlike the other nitrided samples. Therefore, this thin layer can be attributed to the deposition of a thin (Cr-Nb) N coating. Also, it can be argued that diffusion of nitrogen has also taken place since the nitrogen concentration didn't reduce to zero immediately after the coating and this can be correlated with XRD data obtained for this sample. (Refer Sec. 3.1).

3.3 Nitrided layer thickness

Cross-section SEM images of CoCrMo samples nitrided at various bias voltages are depicted in Figure 3a-e. The formation of both compound and diffusion layers can be clearly seen in HLPPN-700V and HLPPN-900V samples whereas HLPPN-1100V and HLPPN-1000V sample showed only a compound layer. The diffusion depth measurements using SEM also showed that the depth increased with increasing bias voltage. Maximum depth of about 3.7 µm was observed for the sample treated with -1100 V followed by 3.3 µm, 1.8 µm and 0.97 µm for -1000 V, - 900 V and - 700 V respectively. EDX analysis (not shown) of these samples showed the absence of target material, Nb in these layers which indicated that these layers are nitrided layers, not (Cr-Nb)N coating.

The sample treated at - 500 V (Fig. 3a) showed a highly dense layer with a unique microstructure as compared to the other samples. EDX analysis of this sample showed that the layer is comprised of Cr, Nb and a small amount of nitrogen. However, it was impossible to establish with EDX that the detected Cr was mainly due to the deposition of (Cr-Nb)N coating as this layer was very thin at approximately 0.97 µm and the substrate also contained a substantial amount of Cr. But the presence of Nb indicated that the deposition of target material has also taken place.

The diffusion depth results are considered an estimation as it is not possible to image the whole diffusion layer using SEM. Nevertheless, these values when further defined by EDX corroborated the findings from XRD and GDOES analysis.

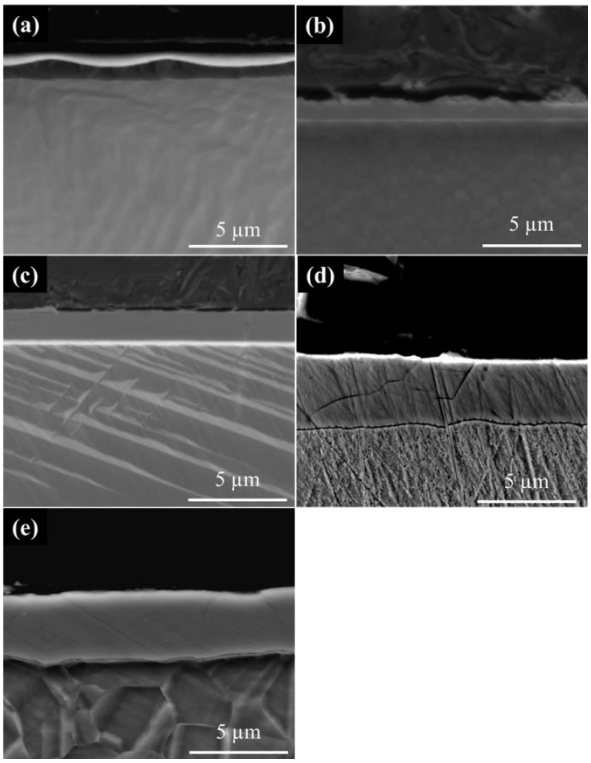

Figure 3: Cross-Section SEM images of nitrided samples at various bias voltages (a) -500 V (b) -700 V (c) -900 V (d) -1000 V and (e) -1100 V

3.4 Microhardness Study

Figure 4 shows the surface microhardness data of untreated and nitrided CoCr samples at various bias voltages. To measure only microhardness of the nitrided layer eliminating the substrate effect, the applied load was kept fixed to 10 g. The surface hardness of treated samples with high bias voltages (from -700 V to -1100 V) increased considerably as compared to untreated CoCr alloy due to the formation of expanded austenite phase. The maximum hardness value of about 2750 ± 9.80 $HK_{0.010}$ at 10 g applied load was observed for the sample treated at -1100 V which was about five orders of magnitude higher that of the untreated sample, 525 ± 2.84 $HK_{0.010}$. The samples treated with -700 V, -900 V and -1000 V exhibited hardness values of 1410 ± 11.76 $HK_{0.010}$, 2230 ± 7.12 $HK_{0.010}$ and 2180 ± 5.56 $HK_{0.010}$ respectively for the same applied load. The increase in

microhardness while increasing the bias voltage could be attributed to the increase in nitriding depth and the compressive stress in (γ_N) phase due to high ion bombardment [14,39,40]. On the other hand, the surface hardness of the sample treated with relatively low bias voltage, -500 V exhibited a very low hardness of 550 ± 3.34 $HK_{0.010}$, even at a low load of 10 g due to the very thin nitrogen diffusion layer at this voltage which allows for substrate hardness interference.

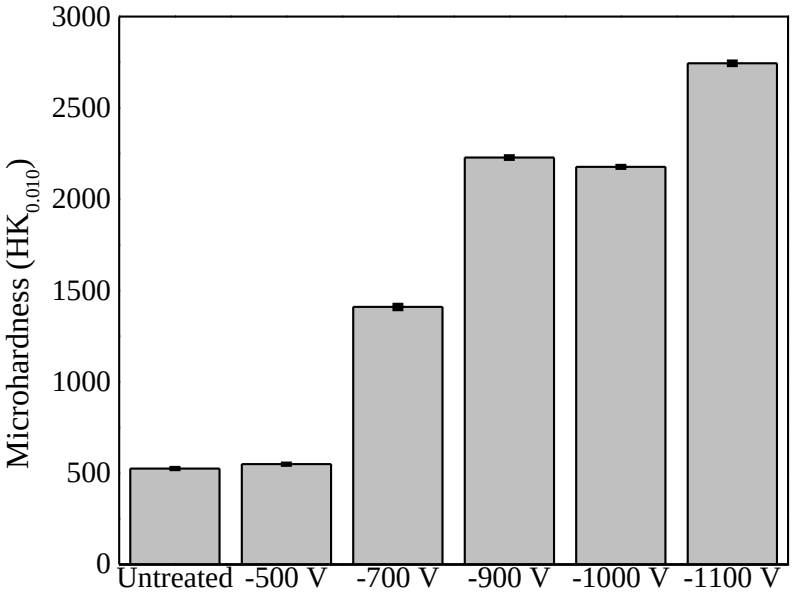

Figure 4: Microhardness value of untreated and nitrided samples at various bias voltages.

3.5 Surface Roughness and Tribological Properties

A Dektak profilometer was used to measure the surface roughness of the samples. As can be seen from Figure 5, the Ra value of the untreated sample was in a range of 15 nm to 20 nm after polishing with (1 µm) diamond slurry. The lowest R_a value of 29 nm was

recorded for the sample that was partially nitrided at -500 V whereas the -1100 V sample showed the highest value of 124 nm. The roughness value of the samples treated with -700 V, - 900 V and -1000 V was found to be 71 nm, 65 nm, and 82 nm respectively. It is important to note that the roughness value increased two-fold while increasing the bias voltage from -900 V to -1100 V. The increase in roughness value can be attributed to the intense bombardment of highly energetic N/H and metal ions at higher bias voltages which produces a significant surface sputtering effect. The roughness will be further influenced by the lattice volume expansion due to the incorporation of Nitrogen into the metallic lattice during the nitriding process. The results summarised in Table 2 clearly demonstrate this trend where the lattice expansion ($\frac{\Delta a}{a_0}$) for both (111) and (200) orientations follows the increase of the nitriding voltage.

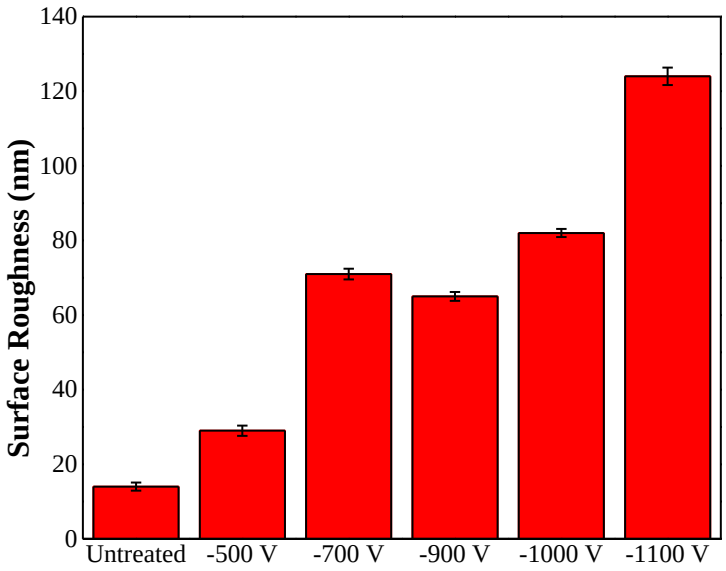

Figure 5: Surface roughness of untreated and nitrided samples various bias voltages.

Figure 6 shows the coefficient of friction (μ) of the nitrided samples at various bias voltages and the untreated sample. The maximum μ value of about 0.8 was recorded for

the untreated sample. Compared to the untreated sample, all the nitrided samples showed a reduced, almost equal μ value of about 0.6, even though the surface roughness of the coatings increased with increasing bias voltage.

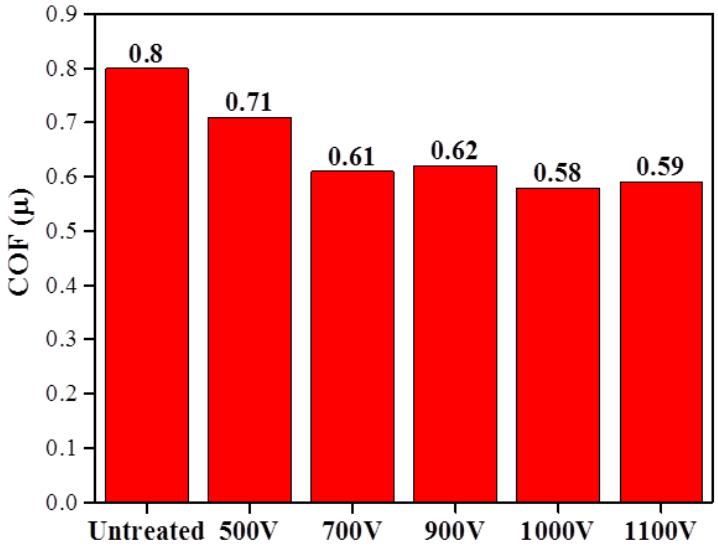

Figure 6: Coefficient of friction of untreated and nitrided samples various bias voltages

A Dektak profilometer was used to profile the wear tracks and calculate the wear volume loss. The wear coefficients (K_C) of treated and untreated samples are shown in Figure 7. The K_C of the partially nitrided sample, -500V showed a very low friction coefficient of 5.58×10^{-16} $m^3N^{-1}m^{-1}$. For the samples treated with high bias voltages (from -700 V to -1100 V), they were found to be in the range of 10^{-15} $m^3N^{-1}m^{-1}$ which was one order of magnitude lower than that of the untreated sample, $K_C = 6 \times 10^{-14}$ $m^3N^{-1}m^{-1}$. The reduction in wear coefficient values clearly demonstrated that the nitriding has significantly increased the wear resistance of CoCrMo alloy. However, among the nitrided samples, the coefficient of wear initially decreased while increasing the bias voltage from -700 V to -900 V before increasing again when the bias voltage was increased to -1000 V. These results showed that increasing the bias voltage beyond - 900

V resulted in deteriorating the wear performance. Generally, it is regarded that a material with high hardness and smooth surface morphology provides better wear resistance. However, it is very well understood that the compressive residual stress in the nitrided layer also increases with hardness due to intense ion bombardment when high bias voltages are used. The high compressive stress can have a detrimental effect on tribological properties such as wear [42]. Therefore, the deterioration in the wear behaviour of samples treated with high bias voltages could be attributed to the high surface roughness and compressive residual stress in the nitrided layers.

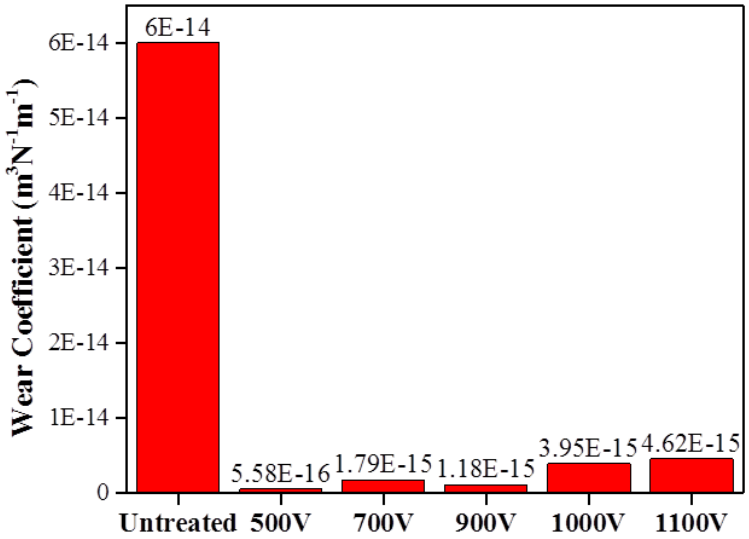

Figure 7: Wear coefficient of untreated and nitrided samples various bias voltages alloy.

4.6 Corrosion performance

The corrosion performance of the untreated CoCrMo alloy and the plasma nitrided specimens was studied using a potentiodynamic polarization test in Hank's solution. Figure 8 shows the polarisation curves obtained from these tests. The corrosion potential E_{corr} can be defined as the potential at which the rate of corrosion reactions

such as oxidation and reduction is exactly equal. When two or more different metal or coating-substrate systems are tested under an identical corrosive environment, the increase in the E_{corr} value of one such system as compared to its counterparts indicates an improvement in the corrosion resistance. The corrosion current density (i_{corr}) is another important parameter showing the kinetics of the above described corrosion reactions. Normally, the corrosion rate is directly proportional to the i_{corr} value. Hence, lower corrosion currents represent better corrosion resistance. Table 3 lists the corrosion potential (E_{corr}) and corrosion current density (i_{corr}) for all the tested specimens.

The E_{corr} value of all the nitrided samples showed a huge increase as compared to the untreated alloy (-775 mV), except for the partially nitrided sample at -500 V which showed relatively small increase (-600 mV). The E_{corr} value increased with increasing bias voltage up to - 900 V before decreasing when the bias voltage was further increased. The highest E_{corr} value of about -220 mV was recorded for the samples nitrided at -700 V and -900 V. These samples showed much reduced i_{corr} values of 7×10^{-3} $mAcm^{-2}$ and 2.40×10^{-3} $mAcm^{-2}$ respectively as compared to 2.10×10^{-2} $mAcm^{-2}$ for the untreated sample. These two samples exhibited a large passivity immediately after the E_{corr} potential in the anodic region, confirming the formation of a passive film. The i_{corr} value of the -900 V sample was almost one order of magnitude lower than that of the untreated sample.

On the contrary, the samples treated at higher bias voltages such as -1000 V and -1100 showed slightly reduced E_{corr} values of -260 mV and -250 mV respectively as compared to HLPPN-700V and HLPPN-900V samples. However, it is important to reiterate that these values are still much higher than that of the untreated alloy. Moreover, these samples exhibited a completely different corrosion behavior with very

high i_{corr} values of 2.3×10^{-2} $mAcm^{-2}$ and 1.60 $mAcm^{-2}$ respectively in the anodic region. The slight decrease in the corrosion potential and high corrosion current could be attributed to the formation of chromium nitride compounds such as CrN and Cr_2N as a result of a high process temperature of about 520 °C due to intense ion bombardment. These chromium nitride compounds inhibited the formation of a Cr_2O_3 passive layer, resulting in high corrosion currents. Similar behavior of high corrosion current and reduced E_{corr} value has already been observed in 316L stainless steel and 470 ferritic steel when the nitriding temperature was increased from 400 °C and 520 °C [43]. It is evident from XRD data also that only HLPPN-1000V and HLPPN-1100V samples contained the chromium nitride compounds as the HLPPN-700V and HLPPN-900V samples showed no peaks for such compounds.

In summary, as compared to the untreated CoCrMo alloy, the noble E_{corr} values and very low i_{corr} values of HLPPN-700V and HLPPN-900V samples showed enhanced corrosion protection after nitriding. Further increase in the bias voltage also exhibited an improvement in the E_{corr} values as compared to the untreated alloy. However, the corrosion currents increased very rapidly in the anodic region due to the formation of chromium nitride compounds, therefore causing deterioration in the corrosion performance. To the best of the authors' knowledge, research articles discussing the corrosion performance of CoCrMo alloy due to nitriding is scarce. The available literatures have mostly shown the deterioration in the corrosion performance of such alloys [31]. In our study, we have demonstrated that the corrosion resistance of the CoCrMo alloy can be improved by plasma nitriding carried out at - 700 V and -900 V bias voltages using HIPIMS technology by avoiding the formation of CrN based compounds.

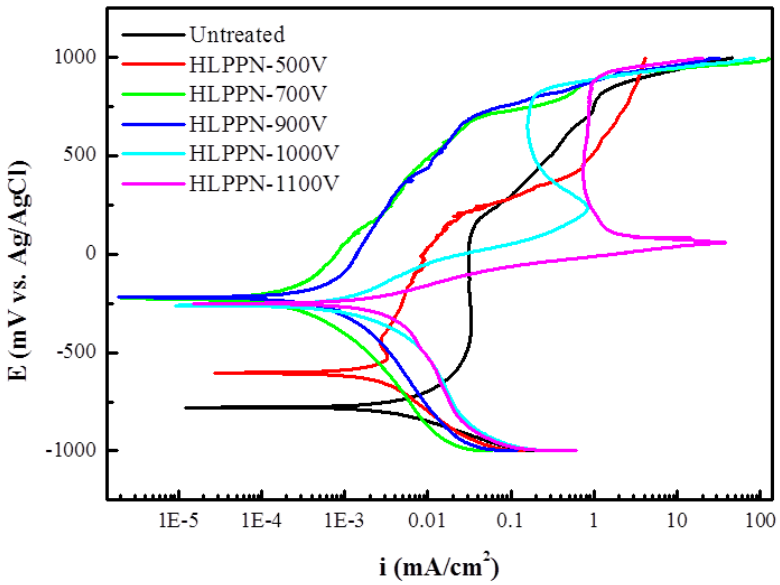

Figure 8: Potentiodynamic polarisation curves obtained in Hank's solution of the untreated CoCrMo alloy and HLPPN at different bias voltage -700 V to -1100 V

Table 2 Corrosion potential and corrosion current denstity values of various samples

Sample	E_{corr} (mV)	I_{corr} (mA/cm^2)
Untreated CoCrMo alloy	-775	2.10×10^{-2}
HLPPN-500V	-600	5.20×10^{-2}
HLPPN-700V	-220	7.00×10^{-3}
HLPPN-900V	-218	2.40×10^{-3}
HLPPN-1000V	-260	2.30×10^{-2}
HLPPN-1100V	-250	1.60

Conclusions

1. Low-pressure plasma nitriding of CoCrMo alloy was successfully carried out in an industrial size coating system using HIPIMS discharge. X ray diffraction analysis of samples treated with high bias voltages (from -700 V to -900 V) revealed the formation of typical expanded austenite phase [γ_N (111) and γ_N (200)] owing to nitriding. Further increase of the nitriding voltage to -1000 V and -1100 V lead to the formation of chromium nitride-based compounds along with the expanded austenite phase due to the intensified ion bombardment and increase in the process temperature. Samples nitrided at a relatively low bias voltage of -500 V showed a deposition of a thin (Cr-Nb)-nitride coating layer due to insufficient re-sputtering and partially nitrided (N solid solution) layer.
2. Texture analysis of the sample treated at UN = -700 V showed that the predominant crystallographic orientation of the nitrided layer was (200) whereas at higher voltages (from -900 V to -1100 V) the layer developed mixed (111) and (200) texture.
3. GDOES measurements of nitrided samples showed that the diffusion depth increased from 1.2 µm to 6 µm while increasing the bias voltage from -700 V to -1100 V.
4. The Knoop microhardness (HK) of nitrided samples was increased by a factor of 5 ($HK_{0.010}$= 2750 ± 9.80 at -1100 V) as compared to the untreated substrate, HK=525, demonstrating the high efficiency of the process.
5. As compared to the untreated sample, the nitrided samples showed one order of magnitude enhanced wear performance. The sample nitrided at -900 V exhibited superior wear resistance ($Kc = 1.18 \times 10^{-15}\ m^3N^{-1}m^{-1}$) with optimum surface roughness (R_a= 65 nm) and hardness (2230 ± 7.12 $HK_{0.010}$) values as compared to its nitrided counterparts and the untreated sample, ($K_C = 6 \times 10^{-14}\ m^3N^{-1}m^{-1}$)

6. The available literatures on corrosion performance of conventionally nitrided CoCrMo alloys have mostly shown deterioration in the corrosion performance of such alloys after the treatment. In this study, we have demonstrated that the corrosion resistance of these alloys can be improved by HIIPIMS plasma nitriding when carried out at - 700 V and -900 V bias voltages by avoiding the formation of CrN based compounds.

Acknowledgement

The authors would like to acknowledge Zimmer-Biomet UK for providing financial support for this research. We would also like to thank Dr. Isabel Lasanta Carrasco of Complutense University of Madrid for her assistance in GDOES measurements and. Mr. Gary Robinson is gratefully appreciated for his technical assistance.

Reference

[1] Y. S. Al Jabbari, "Physico-mechanical properties and prosthodontic applications of Co-Cr dental alloys: a review of the literature," *J. Adv. Prosthodont.*, 2014.

[2] M. A. Hussein, A. S. Mohammed, and N. Al-Aqeeli, "Wear characteristics of metallic biomaterials: A review," *Materials*. 2015.

[3] D. R. Bijukumar *et al.*, "Systemic and local toxicity of metal debris released from hip prostheses: A review of experimental approaches," *Nanomedicine Nanotechnology, Biol. Med.*, vol. 14, no. 3, pp. 951–963, 2018.

[4] F. Guillemot, "Recent advances in the design of titanium alloys for orthopedic applications," *Expert Review of Medical Devices*, vol. 2, no. 6. pp. 741–748, 2005.

[5] X. Luo, X. Li, Y. Sun, and H. Dong, "Tribocorrosion behavior of S-phase surface engineered medical grade Co-Cr alloy," *Wear*, vol. 302, no. 1–2, pp. 1615–1623, 2013.

[6] S. Pramanik, A. K. Agarwal, and K. N. Rai, "Chronology of Total Hip Joint Replacement and Materials Development," vol. 19, no. 1, pp. 15–26, 2005.

[7] O. O'Dwyer Lancaster-Jones, S. Williams, L. M. Jennings, J. Thompson, G. H. Isaac, J. Fisher, M. Al-Hajjar, "Anin vitrosimulation model to assess the severity of edge loading andwear, due to variations in component positioning in hip jointreplacements" J. Biomed. Mater. Res. - Part B Appl. Biomater. 106 (2018) 1897–1906. https://doi.org/10.1002/jbm.b.33991.

[8] S. Virtanen, I. Milošev, E. Gomez-Barrena, R. Trebše, J. Salo, and Y. T. Konttinen, “Special modes of corrosion under physiological and simulated physiological conditions,” *Acta Biomater.*, vol. 4, no. 3, pp. 468–476, 2008.

[9] A. J. Smith, P. Dieppe, K. Vernon, M. Porter, A. W. Blom, and N. Joint, “Failure rates of stemmed metal-on-metal hip replacements : analysis of data from the National Joint Registry of England and Wales,” *Lancet*, vol. 379, no. 9822, pp. 1199–1204.

[10] S. J. Macdonald, “Can a Safe Level for Metal Ions in Patients With Metal-on-Metal Total Hip Arthroplasties Be Determined ?,” vol. 19, no. 8, pp. 71–77, 2004.

[11] M. A. Germain *et al.*, “Comparison of the cytotoxicity of clinically relevant cobalt – chromium and alumina ceramic wear particles in vitro,” vol. 24, pp. 469–479, 2003.

[12] J. Lutz, C. Díaz, J. A. García, C. Blawert, and S. Mändl, “Corrosion behaviour of medical CoCr alloy after nitrogen plasma immersion ion implantation,” *Surf. Coatings Technol.*, 2011.

[13] X. Y. Li, N. Habibi, T. Bell, and H. Dong, “Microstructural characterisation of a plasma carburised low carbon Co–Cr alloy,” *http://dx.doi.org/10.1179/174329407X161564*, vol. 23, no. 1, pp. 45–51, 2013.

[14] H. Dong, “S-phase surface engineering of Fe-Cr, Co-Cr and Ni-Cr alloys,” *Int. Mater. Rev.*, vol. 55, no. 2, pp. 65–98, 2010.

[15] J. Lutz and S. Mändl, “Effect of ion energy and chemistry on layer growth processes during nitriding of CoCr alloys,” *Nucl. Instruments Methods Phys. Res. Sect. B Beam Interact. with Mater. Atoms*, 2009

[16] X. Y. Li, N. Habibi, T. Bell, and H. Dong, “Microstructural characterisation of a plasma carburised low carbon Co–Cr alloy”, Surface Engineering, 23:1, 45-51, Online published: 19 Jul 2013.

[17] Z. L. Zhang, T. Bell, Z. L. Zhang, and T. Bell, “STRUCTURE AND CORROSION RESISTANCE OF PLASMA NITRIDED STAINLESS STEEL,” vol. 0844, 2013.

[18] D. H. and L. C. X. Bell T., “Plasma surface treatment of Co-Cr biomaterial”, European Patent: EP 1 499 755B1.

[19] R. Hutchings and W. C. Oliver, “A study of the improved wear performance of nitrogen-implanted Ti-6Al-4V,” *Wear*, vol. 92, no. 1, pp. 143–153, 1983.

[20] R. Wei, T. Booker, C. Rincon, and J. Arps, “High-intensity plasma ion nitriding of orthopedic materialsPart I. Tribological study,” *Surf. Coatings Technol.*, vol. 186, no. 1–2, pp. 305–313, 2004.

[21] A. You, M. A. Y. Be, and I. In, “Effect of hydrogen and oxygen on stainless steel nitriding,” vol. 764, no. December 2001, 2005.

[22] M. P. Fewell, J. M. Priest, M. J. Baldwin, G. A. Collins, and K. T. Short, “Nitriding at low temperature,” *Surf. Coat. Technol.*, vol. 131, pp. 284–290, 2000.

[23] S. Kumar *et al.*, “The effect of hydrogen on the growth of the nitrided layer in r . f . -plasma-nitrided austenitic stainless steel AISI 316,” *Scan. Electron Microsc.*, vol. 123,

pp. 29–35, 2000.

[24] R. Gu, M. Betzl, I. Alphonsa, B. Ganguly, P. I. John, and S. Mukherjee, “Plasma-source ion implantation compared with glow-discharge plasma nitriding of stainless steel,” vol. 112, pp. 307–309, 1999.

[25] A.P. Ehiasarian, R.Tietema, R. Bugyi, A. Klimczak, P. Eh. Hovsepian, D. Doerwald. A vacuum treatment apparatus, a bias power supply and a method of operating a vacuum treatment apparatus, Patent ZL200780012990.9 in China, granted 10.04.2011, priority date 10.04. 2007. “GB2437080-20071017-Publication document.pdf.” .

[26] A. P. Ehiasarian, P. Eh. Hovsepian, W.-D. Münz, “A Combined Process Comprising Magnetic Field-Assisted, High-Power, Pulsed Cathode Sputtering and an Unbalanced Magnetron”Granted: US 10718435, 2005, EP 1 260 603 A2, DE 10124749, 21.05. 2001.

[27] J. A. Phys, “Interface microstructure engineering by high power impulse magnetron sputtering for the enhancement of adhesion,” vol. 054301, no. March 2007,

[28] Lewis, D. B., et al. (1999). The influence of the yttrium content on the structure and properties of Ti1−x−y−zAlxCryYzN PVD hard coatings. Surface and coatings technology, 114 (2–3), 187-199.

[29] Q. Wang, X. Zhang, C. Huang, and Y. Luo, “Ion Nitriding CoCrMo Alloy for Orthopedic Applications Studied by X-Ray Photoelectron Spectroscopy Analysis and Tribocorrosion Behavior,” *J. Tribol.*, vol. 139, no. 1, p. 011104, 2016.

[30] Surface chemistry and microstructure of metallic biomaterials for hip and knee endoprostheses, Monika Jenko, Matevz Gorensek, Matjaz Godec, Maxinne Hodnik, Barbara Setina Batic, Crtomir Donik, John T. Grant, Drago Dolinar, Applied Surface Science 427 (2018) 584–593.

[31] Tribological and corrosion testing of surface engineered surgical grade CoCrMo alloy**,** J.A.Ortega-Saenz, M.A.L.Hernandez-Rodriguez, V.Ventura-Sobrevilla, R.Michalczewski, J.Smolik, M.Szczerek, Wear 271 (2011) 2125– 2131.

[32] O. Öztürk, S. Okur, and J. P. Riviere, “Structural and magnetic characterization of plasma ion nitrided layer on 316L stainless steel alloy,” *Nucl. Instruments Methods Phys. Res. Sect. B Beam Interact. with Mater. Atoms*, 2009.

[33] M. Berg *et al.*, “On plasma nitriding of steels,” *Surf. Coatings Technol.*, vol. 124, no. 1, pp. 25–31, 2000.

[34] B. Predel, “Co-N (Cobalt-Nitrogen),” in *Ca-Cd -- Co-Zr*, O. Madelung, Ed. Berlin, Heidelberg: Springer Berlin Heidelberg, 1993, pp. 1–3.

[35] P. Hovsepian, G. Thompson. B. Lewis, A. Ehiasarian, and W.-D. Munz, *Performance of High-Precision Knife Blades Treated by Plasma Nitriding and PVD Coating*. 2003.

[36] D. L. Williamson, “No Titl,” in *Mat. Res. Soc. Symp/ Proc.*, 1992, p. 473.

[37] A. Petraitienė, “The Modeling of Nitrogen Mass Transport in CoCr Alloys,” *JELGAVA*

ISSN Rural Sustain. Res., vol. 36, no. 36331, 2016.

[38] S. Parascandola, W. Möller, and D. L. Williamson, "The nitrogen transport in austenitic stainless steel at moderate temperatures," *Appl. Phys. Lett.*, vol. 76, no. 16, pp. 2194–2196, 2000.

[39] T. Balusamy, T. S. N. S. Narayanan, K. Ravichandran, I. S. Park, and M. H. Lee, "Plasma nitriding of AISI 304 stainless steel: Role of surface mechanical attrition treatment," *Mater. Charact.*, vol. 85, pp. 38–47, 2013.

[40] A. Çelik, Ö. Bayrak, A. Alsaran, I. Kaymaz, and A. F. Yetim, "Effects of plasma nitriding on mechanical and tribological properties of CoCrMo alloy," *Surf. Coatings Technol.*, vol. 202, no. 11, pp. 2433–2438, 2008.

[41] T. Christiansen and M. A. J. Somers, "Characterisation of low temperature surface hardened stainless steel," *J. Mater.*, vol. 9, pp. 1–17, 2006.

[42] P. Eh. Hovsepian, D. B. Lewis, W.-D. Münz, Recent Progress in Large Scale Manufacturing of Multilayer/Superlattice Hard Coatings, Surface and Coatings Technology, 133-134 (2000), p. 166-175.

[43] Effect of ionic plasma nitriding process on the corrosion and micro-abrasive wear behavior of AISI 316L austenitic and AISI 470 super-ferritic stainless steels, Elieser de Araújo Junior, Rafael Marinho Bandeira, Marcos Dorigão Manfrinato, Jéferson Aparecido Moreto, Roger Borges, Sandra dos Santos Vales, Paulo Atsushi Suzuki, Luciana Sgarbi Rossino, J MATER RES TECHNOL., 2019; 8(2): 2180-2191.